

**TWO FERROMAGNETIC STATES
IN MAGNETORESISTIVE MANGANITES
- FIRST ORDER TRANSITION DRIVEN BY ORBITALS -**

S. Maekawa, S. Ishihara and S. Okamoto

Institute for Materials Research, Tohoku University, Sendai 980-8577, Japan

(July 26, 1998)

Abstract

A systematic study of the electronic structure in perovskite manganites is presented. The effective Hamiltonian is derived by taking into account the degeneracy of e_g orbitals and strong electron correlation in Mn ions. The spin and orbital orderings are examined as functions of carrier concentration in the mean-field approximation applied to the effective Hamiltonian. We obtain the first order phase transition between ferromagnetic metallic and ferromagnetic insulating states in the lightly doped region. The transition is accompanied with the orbital order-disorder one which is directly observed in the anomalous X-ray scattering experiments. The present investigation shows a novel role of the orbital degree of freedom on metal-insulator transition in manganites.

I. INTRODUCTION

Perovskite manganites have recently attracted much attention. They exhibit a variety of anomalous phenomena such as colossal magnetoresistance (CMR) [1–4] and charge ordering/melting transitions [5,6], which depend crucially on carrier-doping. In this paper, we examine a systematic study of the electronic structure and discuss the mechanism of the properties. An effective Hamiltonian is derived by taking into account the degeneracy of e_g orbitals, strong electron correlation and Hund coupling in Mn ions [7]. In the Hamiltonian, charge, spin and orbital degrees of freedom are included on an equal footing. The spin and orbital orderings are examined as functions of carrier concentration in the mean-field approximation applied to the effective Hamiltonian. We obtain the first order phase transition between ferromagnetic metallic and ferromagnetic insulating states in the lightly doped region. The transition is accompanied with the orbital order-disorder one. We show theoretically how to observe the orbital ordering by the anomalous X-ray scattering.

In Sec. 2, the effective Hamiltonian is derived and examined in the mean-field approximation. We obtain the phase diagram as a function of carrier-doping. In Sec. 3, the anomalous X-ray scattering is discussed as a probe to observe the orbital ordering. The first-order phase transition between two ferromagnetic states is discussed in the light of the phase diagram in Sec. 4. In Sec. 5, the summary and conclusion are given. The present investigation shows a novel role of the orbital degree of freedom on metal-insulator transition in manganites.

II. EFFECTIVE HAMILTONIAN AND PHASE DIAGRAM

Let us start with undoped perovskite manganites such as LaMnO_3 , where each Mn^{3+} ion has one e_g and three t_{2g} electrons. The e_g electron occupies one of the orbitals $d_{3z^2-r^2}$ and $d_{x^2-y^2}$ as shown in Fig. 1, and couples with the localized t_{2g} spins ferromagnetically due to the Hund coupling. The Hund coupling and the antiferromagnetic exchange interaction

between nearest-neighbor t_{2g} spins are given by

$$H_K + H_{t_{2g}} = -K \sum_i \vec{S}_i^{t_{2g}} \cdot \vec{S}_i + J_s \sum_{\langle ij \rangle} \vec{S}_i^{t_{2g}} \cdot \vec{S}_j^{t_{2g}} , \quad (1)$$

where both the constants K and J_s are defined to be positive, and $\vec{S}_i^{t_{2g}}$ and \vec{S}_i are the operators for a t_{2g} spin with $S=3/2$ and that of e_g electron with $S=1/2$, respectively. The two e_g orbitals are assumed to be degenerate. The matrix elements of the electron transfer between γ orbital at site i and γ' orbital at nearest neighbor site j , $t_{ij}^{\gamma\gamma'}$, is estimated by the second-order perturbation with respect to the electron transfer between $Mn3d$ and $O2p$ orbital (t_{pd}). t_{pd} is parameterized as $t_{pd} = \alpha(\gamma)V_{pd\sigma}$, where α is a numerical factor and $V_{pd\sigma}$ is an overlap integral independent of the orbitals. Then, $t_{ij}^{\gamma\gamma'}$ is denoted by $t_{ij}^{\gamma\gamma'} = \alpha(\gamma)\alpha(\gamma')t_0$, where $t_0(\propto V_{pd\sigma}^2)$ is treated as a parameter. The strong intra- and inter-orbital Coulomb interactions U and U' , respectively, cause the localization of e_g electrons. We eliminate the doubly occupied configuration in the e_g states and obtain the leading term of the effective Hamiltonian [7],

$$H_{eff} = \widetilde{H}_{e_g} + H_K + H_{t_{2g}} , \quad (2)$$

with

$$\widetilde{H}_{e_g} = -2\tilde{J} \sum_{\langle ij \rangle} \left(\frac{3}{4} + \vec{S}_i \cdot \vec{S}_j \right) \left(\frac{1}{4} - \psi_i^\dagger \hat{\tau}_{ij} \psi_j \right) , \quad (3)$$

where

$$\psi_i^\dagger = (T_i^z, T_i^x) , \quad (4)$$

$$\hat{\tau}_{ii+l} = \frac{1}{2} \begin{pmatrix} 1 + \cos n_l \frac{2\pi}{3} & \sin n_l \frac{2\pi}{3} \\ \sin n_l \frac{2\pi}{3} & 1 - \cos n_l \frac{2\pi}{3} \end{pmatrix} \quad (5)$$

with $(n_x, n_y, n_z) = (1, 2, 3)$. Here, $\tilde{J} = t_0^2/(U' - J)$ with $J'(> 0)$ being the intra-orbital exchange interaction between e_g electrons. \vec{T}_i is the pseudo-spin operator for the orbital degree of freedom at site i defined as

$$\vec{T}_i = \frac{1}{2} \sum_{\sigma\gamma\gamma'} \tilde{d}_{i\gamma\sigma}^\dagger \vec{\sigma}_{\gamma\gamma'} \tilde{d}_{i\gamma'\sigma} , \quad (6)$$

where $\vec{\sigma}$ is the Pauli matrix and $\tilde{d}_{i\gamma\sigma} = d_{i\gamma\sigma}(1 - n_{i\gamma-\sigma})(1 - n_{i-\gamma\sigma})(1 - n_{i-\gamma-\sigma})$ with $d_{i\gamma\sigma}$ being the annihilation operator of an electron with spin σ in the orbital γ at site i and $n_{i\gamma\sigma} = d_{i\gamma\sigma}^\dagger d_{i\gamma\sigma}$. The eigenstates of the operator \vec{T}_i correspond to the occupied and unoccupied e_g orbitals. For example, for the $T^z = 1/2$ and $-1/2$, an electron occupies the $d_{3z^2-r^2}$ and $d_{x^2-y^2}$ orbitals, respectively. We note that Eq. (3) does not include T^y .

In the doped manganites such as $\text{La}_{1-x}\text{Sr}_x\text{MnO}_3$, eg electrons have the kinetic energy,

$$H_t = \sum_{\langle ij \rangle \sigma \gamma \gamma'} (t_{ij}^{\gamma\gamma'} \tilde{d}_{i\gamma\sigma}^\dagger \tilde{d}_{i\gamma\sigma'} + h.c.) . \quad (7)$$

A similar model Hamiltonian with Eq. (3) has been proposed by Khomskii and Kugel [8] and Castellani, Natoli and Ranninger [9]. However, effects of t_{2g} spins were not introduced in their model. Roth [10], Cyrot and Lyon-Caen [11] and Inagaki [12] also proposed a model, which coincides with ours if the matrix elements of the electron transfer are assumed as $t_{ij}^{\gamma\gamma'} = t_0 \delta_{\gamma\gamma'}$. In this case, the orbital interaction is isotropic in contrast with Eq. (3).

The Hund coupling K is so strong that e_g and t_{2g} spins at the same site are parallel. As seen in Eq. (3), spins prefer ferromagnetic ordering, whereas orbitals do the alternate ordering which is called the antiferro-type, hereafter. It is known that in the doped manganites, the carrier motion induces spin ferromagnetism due to the double exchange interaction. Therefore, we may expect a rich phase diagram as a function of the parameters, and as well as carrier concentration.

We obtain the phase diagram at zero temperature as a function of hole concentration and in the mean field approximation [13] applied to the effective Hamiltonian. In the spin and orbital structures, four types of the mean field are considered; the ferro (F)-type, and three antiferro-types (layer(A)-type, rod(C)-type and NaCl(G)-type). We introduce the rotating frame in the spin and orbital spaces [14] and describe the states by the rotating angle $\theta_i^{(s)}$ and $\theta_i^{(t)}$, respectively. In the rotating frame, $\langle \tilde{S}_i^z \rangle (= \cos \theta_i^{(s)} \langle S_i^z \rangle - \sin \theta_i^{(s)} \langle S_i^x \rangle)$, and $\langle \tilde{T}_i^z \rangle (= \cos \theta_i^{(t)} \langle T_i^z \rangle - \sin \theta_i^{(t)} \langle T_i^x \rangle)$, are adopted as the mean field order parameters. The kinetic energy term (H_t) is rewritten as $-\sum_{\langle ij \rangle} h_j^\dagger h_i \sum_{\sigma} z_{i\sigma}^{(s)*} z_{j\sigma}^{(s)} \sum_{\gamma\gamma'} z_{i\gamma}^{(t)*} t_{ij}^{\gamma\gamma'} z_{j\gamma'}^{(t)} + h.c.$, where h_i is a fermion operator describing the hole carrier and $z_{i\sigma}^{(s)} (z_{i\gamma}^{(t)})$ is the element of

the unitary matrix for the rotation in the spin (orbital) frame. We assume $\langle h_i^\dagger h_i \rangle = x$ and represent $\langle z_{i\sigma}^{(s)*} z_{i\sigma}^{(s)} \rangle$ and $\langle z_{i\gamma}^{(t)*} t_{ij}^{\gamma\gamma'} z_{i\gamma'}^{(t)} \rangle$ by the rotating angle. By minimizing the energy, the phase diagram at $T = 0$ is obtained.

The results are shown in Fig. 2. The value of J_s/t_0 in the manganites which we are interested in is estimated to be $0.001 \sim 0.01$ from the Neel temperature of CaMnO_3 [15]. Therefore, let us consider the case with $J_s/t_0 = 0.004$. At the hole concentration $x = 0.0$, the A-type antiferromagnetic spin ordering is realized. With increasing x , the ferromagnetic spin state appears where the orbitals show the ordering given in Fig. 3 (a). This state is called F_1 . With further increasing x , we find the phase separation between two ferromagnetic spin states F_1 and F_2 . The state F_2 shows the orbital ordering given in Fig. 3 (b) which provides the gain of the kinetic energy of hole carriers. Since the state has more holes than F_1 , the ferromagnetism in the state F_2 is caused by the double exchange interaction. On the other hand, the state F_1 has less holes and the ferromagnetism is due to the superexchange interaction induced by the orbital antiferro-type ordering. In Fig. 4, the total energy is plotted as a function of x . The two minima correspond to F_1 and F_2 . For example, the compound with $x = 0.2$ shows the phase separation, and 60% and 40% of the sample are F_1 with $x = 0.06$ and F_2 with $x = 0.41$, respectively. Recently, the first-order phase transition between two ferromagnetic spin states has been experimentally observed. The details will be discussed in Sec. 4. Fig. 2 also shows the phase separation between A-type and C-type antiferromagnetic states when is large. Such a phase separation may be realized in the materials with small hopping parameter t . The two ferromagnetic states have also been shown by Maezono *et al.* [16] The results are in accord with ours although the theoretical method is different each other. Yunoki *et al.* [17] have proposed the phase separation between two ferromagnetic states due to the Jahn-Teller coupling without electron correlation.

III. ORBITAL ORDERING AND ANOMALOUS X-RAY SCATTERING

As discussed in the previous section, the orbital ordering plays a crucial role in the magnetic and electronic properties in manganites. However, the direct observation of the orbitals was limited experimentally. Recently, Murakami *et al.* have applied the anomalous X-ray scattering in order to detect the orbital ordering in single layered manganites $\text{La}_{0.5}\text{Sr}_{1.5}\text{MnO}_4$ [18]. They focused on a reflection at $(3/4, 3/4, 0)$ point and obtained a resonant-like peak near the K-edge of a Mn^{3+} ion below about 200K. They further observed the unique polarization dependence which is attributed to the tensor character of the anomalous scattering factor. When all Mn^{3+} ions are equivalent, the reflection at $(3/4, 3/4, 0)$ is forbidden. Therefore, an appearance of the intensity implies that two kinds of orbital are alternately aligned in the MnO_2 plane (antiferro-type). The experimental results also imply that the dipole transition between Mn $1s$ and Mn $4p$ orbitals causes the scattering. The experimental method was extended to $\text{La}_{1-x}\text{Sr}_x\text{MnO}_3$ with $x = 0.0$ [19] and 0.12 [20]. In this section, we study theoretically the anomalous X-ray scattering in relation to its role as a detector of the orbital ordering in manganites [21].

The structure factor of the X-ray scattering is expressed as a sum of the normal and anomalous part of the atomic scattering factor. The normal part is given by the Fourier transform of the charge density ρ_i in the i -th atom, $f_{0i} = \langle f | \rho_i(\vec{K} = \vec{k}'' - \vec{k}') | 0 \rangle$, where $|0\rangle(|f\rangle)$ is the initial (final) electronic state with energy ε_0 (ε_f), and \vec{k}' and \vec{k}'' are the momenta of incident and scattered photons, respectively. The anomalous part is derived by the interaction between electronic current and photon and is expressed as

$$\Delta f_{i\alpha\beta} = \frac{m}{e^2} \sum_i \left(\frac{\langle f | j_{i\alpha}(-\vec{k}') | l \rangle \langle l | j_{i\beta}(\vec{k}'') | 0 \rangle}{\varepsilon_0 - \varepsilon_l - \omega_{k''} - i\delta} + \frac{\langle f | j_{i\beta}(\vec{k}'') | l \rangle \langle l | j_{i\alpha}(-\vec{k}') | 0 \rangle}{\varepsilon_0 - \varepsilon_l + \omega_{k'} - i\delta} \right), \quad (8)$$

where $|l\rangle$ is the intermediate electronic states with energy ε_l and δ is a dumping constant. The current operator $j_{i\alpha}(\vec{k})$ describes the dipole transition between Mn $1s$ and $4p$ orbitals at site i coupled with photon with polarization in the α direction. The contribution from the quadrupole transition is neglected because the inversion symmetry is preserved in the system which we are interested in.

As mentioned above, the anomalous scattering is dominated by the Mn $1s \rightarrow 4p$ E1 transition. In this case, how does the $3d$ orbital ordering reflect on the anisotropy of the anomalous scattering factor? In order to study the problem, we consider the electronic structure in a MnO_6 octahedron, since the local electronic excitation dominates. Then, we find that the electron hybridization do not result in the anisotropy of the scattering factor, since the hybridization between the Mn $3d$ and O $2p$ orbitals and between the Mn $4p$ and O $2p$ ones are decoupled. One of the promising origins of the anisotropy of the scattering factor is the Coulomb interaction between Mn $3d$ and $4p$ electrons. The electron-electron interaction in the orbital ordered state breaks the cubic symmetry and thus lifts the degeneracy of Mn $4p$ orbitals.

The interaction between Mn $3d$ and $4p$ electrons is represented as

$$V(3d_{\gamma\theta\pm}) = F_0 + 4F_2 \cos\left(\theta \pm m_\gamma \frac{2\pi}{3}\right), \quad (9)$$

where $m_x = +1$, $m_y = -1$, and $m_z = 0$, and $|3d_{\gamma\theta+}\rangle = \cos(\theta/2)|3z^2 - r^2\rangle + \sin(\theta/2)|x^2 - y^2\rangle$ and $|3d_{\gamma\theta-}\rangle$ is its counterpart. F_n is the Slater integral between $3d$ and $4p$ electrons. The explicit formula of F_n is given by $F_0 = F^{(0)}$ and $F_2 = F^{(2)}/35$ with $F^{(n)} = \int dr dr' r^2 r'^2 R_{3d}(r)^2 R_{4p}(r')^2 \frac{r_{<}^n}{r_{>}^{n+1}}$, where $r_{<}$ ($r_{>}$) is the smaller (larger) one between r and r' . When $d_{3z^2-r^2}$ orbital is occupied ($\theta = 0$), the energy in the $4p_z$ orbital is higher than that of the $4p_x$ ($4p_y$) orbital by $6F_2$. As a result, $(\Delta f_i)_{xx(yy)}$ dominates the anomalous scattering near the edge in comparison with $(\Delta f_i)_{zz}$.

The inter atomic Coulomb interaction between Mn $4p_\gamma$ electron and O $2p_{\gamma\theta-}$ hole also provides an origin of the anisotropy of the scattering factor through the Mn $3d$ -O $2p$ hybridization. The interaction is represented by $V(2p_{\gamma\theta-}, 4p_\gamma) = -\varepsilon + \frac{\varepsilon\rho^2}{5} \cos(\theta + m_\gamma \frac{2\pi}{3})$, where the definition of m_γ is the same as that in Eq. (9). $\varepsilon = Ze^2/a$ and $\rho = \langle r_{4p} \rangle / a$, where $Z = 2$, a is the Mn-O bond length, and $\langle r_{4p} \rangle$ is the average radius of Mn $4p$ orbital. Although the above two interactions cooperate to bring about the anisotropy of the scattering factor, it seems likely that the magnitude of $V(2p_{\gamma\theta-}, 4p_\gamma)$ is much reduced by the screening effects in comparison with $V(3d_{\gamma\theta+}, 4p_\gamma)$.

Being based on the Hamiltonian, the imaginary part of the scattering factor is calculated by the configuration interaction method. The calculated $(\Delta f_i)_{\alpha\alpha}$ near the K-edge is shown in Fig. 5 (a), where the $d_{3z^2-r^2}$ orbital is occupied. It is noted that the edge of the lowest main peak corresponds to the Mn K-edge. The detailed structure away from the edge may become broad and be smeared out in the experiments by overlapping with other peaks which are not included in the calculation. In the figure, the scattering intensity is governed by $(\Delta f_i)_{xx}$. Owing to the core hole potential, main and satellite peaks are attributed to the transition from the ground state, which is mainly dominated by the $|3d_{\gamma\theta+}^1\rangle$ state, to the $|\underline{1s}3d_{\gamma\theta+}^1 3d_{\gamma\theta-}^1 4p_{x(z)}^1 \underline{2p_{\gamma\theta-}}\rangle$ and $|\underline{1s}3d_{\gamma\theta+}^1 4p_{x(z)}^1\rangle$ excited states, respectively, where the underlines show the states occupied by holes, although the two excited states strongly mix with each other. Therefore, the anisotropy in the main peak is caused by $V(3d_{\gamma\theta+}, 4p_{\gamma})$ through the Mn $3d$ -O $2p$ hybridization. As a comparison, the results in the case where the $d_{x^2-y^2}$ orbital is occupied are shown in Fig. 5 (b). In the figure, the anisotropy near the edge is entirely opposite to that in Fig. 5 (a); i.e., the scattering factor near the edge is governed by $(\Delta f_i'')_{zz}$, owing to the positive value of $V(3d_{x^2-y^2}, 4p_x) - V(3d_{x^2-y^2}, 4p_z)$.

IV. FIRST ORDER TRANSITION BETWEEN TWO FERROMAGNETIC STATES

Recently, the first-order phase transition between ferromagnetic metallic and ferromagnetic insulating states has been discovered in $\text{La}_{1-x}\text{Sr}_x\text{MnO}_3$ with $x \sim 0.12$ [20]. In this section, we discuss the transition in the light of the phase diagram given in Sec. 2. Let us first review the experimental data. The electrical resistivity $\rho(T)$ shows an anomalous temperature dependence below the Curie temperature $T_C = 170\text{K}$. It is metallic between T_C and $T_L = 145\text{K}$. However, as temperature decreases below T_L , ρ increases rapidly and the crystal structure changes to the less distorted (pseudo cubic) O^* phase from the distorted orthorhombic O' phase [22]. A first-order transition occurs by applying a magnetic field between T_C and T_L . Discontinuous jump in both ρ and the magnetization curve are brought

about at the critical field $H_C(T)$. The striction ΔL defined as $\Delta L = L(T) - L(140K)$ tends to zero above $H_C(T)$. With decreasing temperature, $H_C(T)$ decreases and at T_C it goes to zero.

The temperature dependence of lattice constant and magnetic Bragg reflection intensity were observed in the neutron scattering experiments. The results are plotted in Fig. 6. The ferromagnetic order parameter jumps at T_C simultaneously with the O' to O^* phase transition upon cooling. Superlattice reflections such as $(h, k, l + 1/2)$ were also observed, indicating the lattice modulation due to the charge ordering, which is consistent with the previous results [23]. The two ferromagnetic phases have different orbital structure. The resonance-like peak appears at the $(0, 3, 0)$ reflection in the anomalous X-ray scattering experiments, when the photon energy is tuned at the K-edge (6.552 KeV) in a Mn^{3+} ion as shown in Fig. 7. Besides the energy scan, the azimuthal scan around the scattering vector shows the angle dependence of two-fold sinusoidal symmetry, which gives rise to a direct evidence of the antiferro-type orbital ordering as that in the undoped system $LaMnO_3$ [19]. We stress the fact that the intensity appears only below $T_L(O^*$ phase), as shown in Fig. 7, where the notable lattice distortion does not exist. Therefore, the antiferro-type orbital ordering is not the one associated with the Jahn-Teller type lattice distortion. Note that the spin-wave dispersion in $La_{0.88}Sr_{0.12}MnO_3$ is nearly isotropic, which is entirely different from the two-dimensional relation in $LaMnO_3$, due to the antiferro-type orbital ordering of $d_{3x^2-r^2}/d_{3y^2-r^2}$, which is shown in Fig. 3 (c). Therefore, we anticipate that $La_{0.88}Sr_{0.12}MnO_3$ should have a different orbital state, e.g. the hybridization of $d_{z^2-x^2}(y^2-z^2)$ and $d_{3x^2-r^2}(3y^2-r^2)$.

We consider that the two ferromagnetic states observed in this compound correspond to F_1 and F_2 in the phase diagram in Fig. 2, and the first-order transition occurs between them by applying magnetic field and/or changing temperature. At high temperatures, the F_2 phase is favorable because the entropy promotes the orbital disordering and carrier mobility. At low temperatures, on the other hand, the F_1 phase becomes dominant and occupies the large volume fraction in the system. The stabilization of F_1 phase by an applied magnetic field is also explained as follows: (1) both ferromagnetic ordering and antiferro-type orbital

ordering are confirmed to be cooperatively stabilized (2) the magnetic moment is enlarged by changing the dominant magnetic coupling from the double exchange interaction to the superexchange interaction. The first-order phase transition from ferromagnetic metallic to ferromagnetic insulating states is ascribed to the simultaneous transition of orbital order-disorder states. The phase separation occurs between these two ferromagnetic phases and the insulating phase dominates the system with increasing the magnetic field and/or decreasing temperature. The present investigations show a novel role of the orbital degree of freedom in the metal-insulator transition as a hidden parameter, unambiguously for the first time.

V. CONCLUSION

We have studied the magnetic and electronic structure in perovskite manganites taking into account the degeneracy of e_g orbitals and strong electron correlation in Mn ions. The spin and orbital orderings were examined as functions of carrier concentration in the mean-field approximation applied to the effective Hamiltonian, which describes the low energy states. We obtained the phase separation between ferromagnetic metallic and ferromagnetic insulating states in the lightly doped region. The two ferromagnetic states have been discovered experimentally in $\text{La}_{1-x}\text{Sr}_x\text{MnO}_3$ with $x \sim 0.12$. The ferromagnetic metallic state is due to the double exchange interaction, whereas the ferromagnetic insulating state is caused by the superexchange interaction coupled with the orbital degree of freedom. The orbital degree of freedom was considered to be a hidden parameter until recently, since the direct observation was much limited experimentally. We have studied theoretically the anomalous X-ray scattering in relation to its role as a probe of the orbital ordering in manganites. We conclude that the orbital degree of freedom is not a hidden parameter but is examined together with spin and charge degrees of freedom of electrons in manganites.

ACKNOWLEDGEMENTS

The work described in Sect. 4 was done in collaboration with Y. Endoh, K. Hirota, T. Fukuda, H. Kimura, H. Nojiri, and K. Kaneko at Tohoku University and Y. Murakami at

KEK. We thank them for providing the experimental data prior to publication and valuable discussions. This work was supported by Priority Areas Grants from the Ministry of Education, Science and Culture of Japan, and CREST (Core Research for Evolutional Science and Technology Corporation) Japan. The numerical calculation was performed at the supercomputer facilities of Institute for Materials Research, Tohoku University and Institute of Solid State Physics, University of Tokyo. S. O. acknowledges the financial support of JSPS Research Fellowship for Young Scientists.

REFERENCES

- [1] K.Chahara, T.Ohono, M.Kasai, Y.Kanke, and Y.Kozono, Appl. Phys. Lett. **62**, 780 (1993).
- [2] R. von Helmholt, J. Wecker, B. Holzapfel, L. Schultz and K. Samwer, Phys. Rev. Lett. **71**, 2331 (1993).
- [3] Y. Tokura, A. Urushibara, Y. Moritomo, T. Arima, A. Asamitsu, G. Kido, and N. Furukawa, Jour. Phys. Soc. Jpn. **63**, 3931 (1994).
- [4] S. Jin, T. H. Tiefel, M. McCormack, R. A. Fastnacht, R. Ramesh, and L. H. Chen, Science, **264**, 413 (1994).
- [5] Z. Jirak, S. Krupicka, Z. Simsa, M. Dlouha, and S. Vratislav, J. Mag. Mat. , **53**, 153 (1985).
- [6] Y. Tomioka, A. Asamitsu, Y. Moritomo, and Y. Tokura, Jour. Phys. Soc. Jpn. **64**, 3626 (1995).
- [7] S. Ishihara, J. Inoue, and S. Maekawa, Physica C 263, 130 (1996), and Phys. Rev. B **55**, 8280 (1997).
- [8] K. I. Kugel, and D. I. Khomskii, ZhETF Pis. Red. —bf 15, 629 (1972). (JETP Lett. **15**, 446 (1972)); D. I. Khomskii, and K. I. Kugel, Sol. Stat. Comm. **13**, 763 (1973).
- [9] C. Castellani, C. R. Natoli, and J. Ranninger, Phys. Rev. B **18**, 4945, (1978); T. M. Rice, in: Spectroscopy of Mott Insulators and Correlated Metals, Springer Series in Solid-State Science, Vol. 119, p. 221, A.Fujimori and Y.Tokura ed., Springer, Berlin, (1998).
- [10] L. M. Roth, Phys. Rev. **149**, 306, (1966).
- [11] M. Cyrot, and C. Lyon-Caen, Le Jour. de Physique **36**, 253 (1975).
- [12] S. Inagaki, Jour. Phys. Soc. Jpn. **39**, 596 (1975).

- [13] S. Ishihara, S. Okamoto, and S. Maekawa, *J. Phys. Soc. Jpn.* **66**, 2965 (1997).
- [14] S. Ishihara, M. Yamanaka, and N. Nagaosa, *Phys. Rev. B* **56**, 686 (1997).
- [15] J. B. Goodenough, in: *Progress in Solid State Chemistry*, H. Reiss ed., Pergamon, London, (1971).
- [16] R. Maezono, S. Ishihara, and N. Nagaosa, *Phys. Rev. B* **57**, R13993 (1998).
- [17] S. Yunoki, A. Moreo, and E. Dagotto, (unpublished, cond-mat/9807149)
- [18] Y. Murakami, H. Kawada, H. Kawata, M. Tanaka, T. Arima, H. Moritomo and Y. Tokura, *Phys. Rev. Lett.* **80**, 1932 (1998).
- [19] Y. Murakami, J. P. Hill, D. Gibbs, M. Blume, I. Koyama, M. Tanaka, H. Kawata, T. Arima, T. Tokura, K. Hirota, and Y. Endoh, *Phys. Rev. Lett.* **81**, 582 (1998).
- [20] Y. Endoh, K. Hirota, Y. Murakami, T. Fukuda, H. Kimura, N. Nojiri, K. Kaneko, S. Ishihara, S. Okamoto, and S. Maekawa , (unpublished).
- [21] S. Ishihara, and S. Maekawa, *Phys. Rev. Lett.* **80**, 3799 (1998).
- [22] H. Kawano, R. Kajimoto, M. Kubota, and H. Yoshizawa, *Phys. Rev. B.* **53**, R14709 (1996).
- [23] Y. Yamada, O. Hino, S. Nohdo, R. Kanao, T. Inami, and S. Katano, *Phys. Rev. Lett.* **77**, 904 (1996).

Figure captions

Fig. 1. Schematic illustration of $d_{3z^2-r^2}$ and $d_{x^2-y^2}$ orbitals in an octahedron of O ions.

Fig. 2: Theoretical phase diagram at zero temperature calculated in the mean field approximation as a function of the carrier concentration (x) and the antiferromagnetic superexchange interaction (J_s) between localized t_{2g} spins. J_s is normalized by t_0 which is the electron transfer intensity between neighboring e_g orbitals in Mn ions, and the realistic value of J_s/t_0 is estimated to be of the order of 0.001 for the Neel temperature of CaMnO_3 . The two kinds of ferromagnetic phases (F_1 and F_2) with different orbital structures are shown and phase separation region $PS(F_1/F_2)$ where F_1 and F_2 coexist with different volume fractions appears between them. A and C imply the layer-type and rod-type antiferromagnetic phases, respectively, and PS implies the phase separated region between ferromagnetic and antiferromagnetic phases, and the two antiferromagnetic phases.

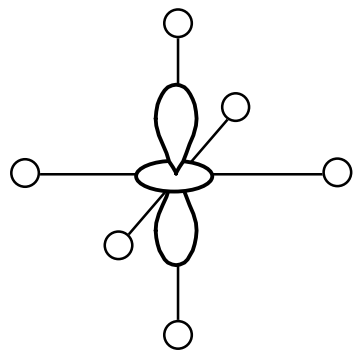
Fig. 3: Schematic illustration of the orbital orderings obtained by the theoretical calculation. (a) ferromagnetic insulating state (F_1) and (b) ferromagnetic metallic state (F_2) given in Fig. 2. The orbital structure in LaMnO_3 is shown in (c) for comparison.

Fig. 4: Total energy of a function of hole concentration x . Two minima correspond to the F_1 and F_2 states.

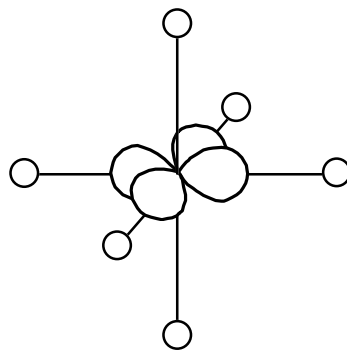
Fig. 5: The imaginary part of the scattering factor $[(\Delta f''_i)_{xx} m / \pi |A_{x(z)}|^2]$ in the case where the following orbital is occupied: (a) $\theta = 0 (d_{3z^2-r^2})$ and (b) $\theta = \pi (d_{x^2-y^2})$. The straight and broken lines show $(\Delta f''_i)_{xx}$ and $(\Delta f''_i)_{zz}$, respectively. The origin of the energy is taken to be arbitrary. Here, m is the mass of an electron and $A_{x(z)}$ is the coupling constant between electron and photon with $x(z)$ polarization of the electric field.

Fig. 6: Temperature dependence of (a) lattice parameter, and (b) integrated intensity of (2 0 0) ferromagnetic Bragg reflection measured with 14.7 meV neutrons. [20] Between $T_L (= 145\text{K})$ and $T_H (= 291\text{K})$, the crystal structure is determined to be O' (orthorhombic). Out side of these temperatures, O^* (pseudo cubic). T_C is determined to be 170 K for $\text{La}_{0.88}\text{Sr}_{0.12}\text{MnO}_3$ which is consistent with the magnetization measurement.

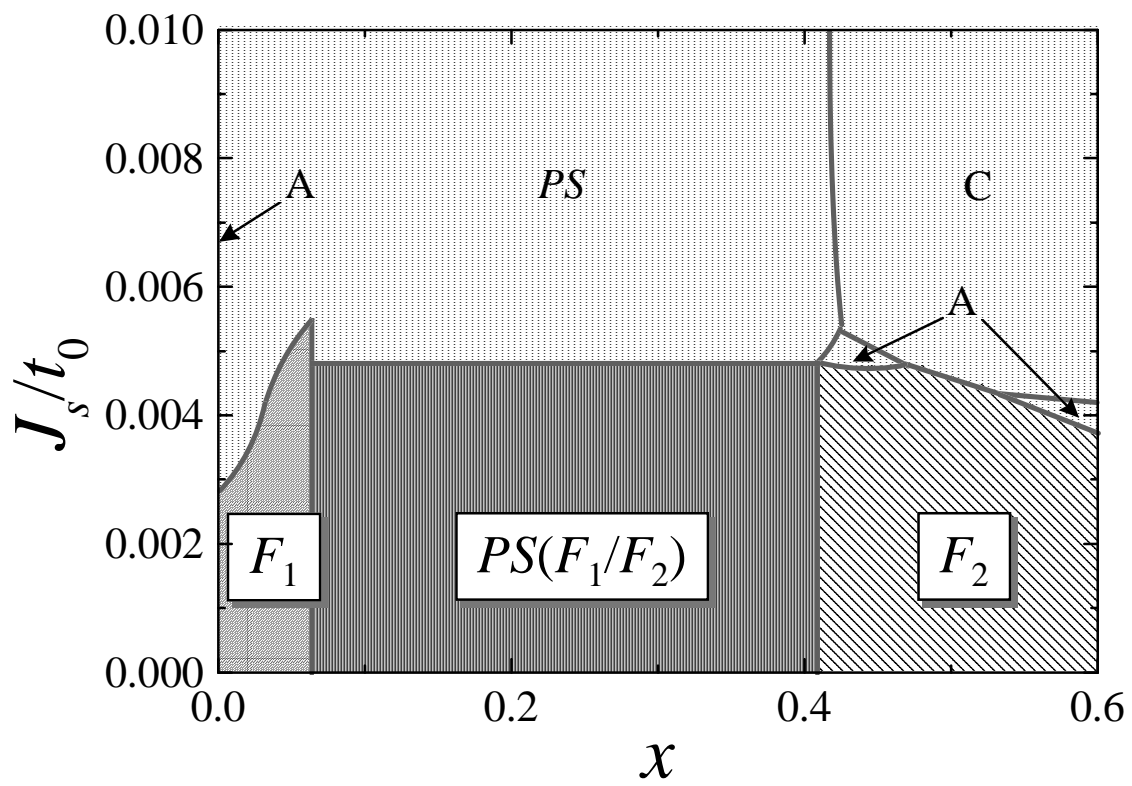
Fig. 7: (a) Energy dependence of intensities in the anomalous X-ray scattering experiments at the orbital ordering reflection $(0\ 3\ 0)$ at $T = 12K$ in $\text{La}_{0.88}\text{Sr}_{0.12}\text{MnO}_3$. [20] The resonant energy is determined to be 6.552 KeV. The dashed curve represents fluorescence showing the resonant energy corresponding to the K-edge of Mn cation. (b) The azimuthal angle dependence of orbital ordering reflection $(0\ 3\ 0)$. The solid line is two-fold squared sine curve of angular dependence. (c) Temperature dependence of peak intensities of orbital ordering reflection $(0\ 3\ 0)$.

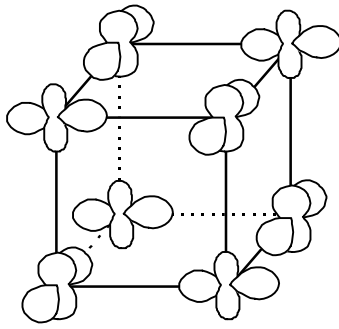


$$d_{3z^2-r^2}$$

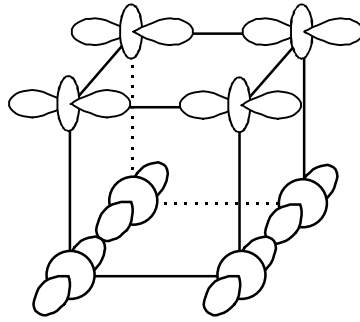


$$d_{x^2-y^2}$$

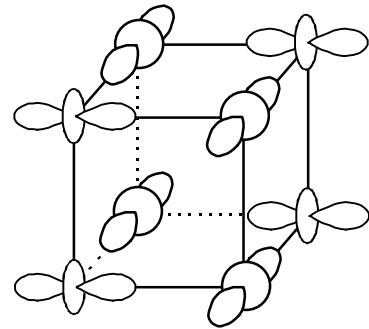




(a)



(b)



(c)

